

NATIONAL AERONAUTICS AND SPACE ADMINISTRATION

*Technical Memorandum No. 33-234**Engineering Models of the Martian
Atmosphere and Surface**D. F. Spencer*

N66 26871

FACILITY FORM 802

(ACCESSION NUMBER)	33
(PAGES)	CP 75236
(NASA CR OR TMX OR AD NUMBER)	

(THRU)	1
(CODE)	30
(CATEGORY)	

jpl

JET PROPULSION LABORATORY
CALIFORNIA INSTITUTE OF TECHNOLOGY
PASADENA, CALIFORNIA

July 1, 1965

GPO PRICE \$ _____

CFSTI PRICE(S) \$ _____

Hard copy (HC) \$2.00

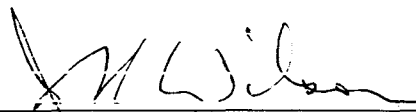
Microfiche (MF) .50

NATIONAL AERONAUTICS AND SPACE ADMINISTRATION

Technical Memorandum No. 33-234

*Engineering Models of the Martian
Atmosphere and Surface*

D. F. Spencer

A handwritten signature in black ink, appearing to read "J. N. Wilson", written over a horizontal line.

J. N. Wilson, Voyager Section Manager
Engineering Mechanics Division

JET PROPULSION LABORATORY
CALIFORNIA INSTITUTE OF TECHNOLOGY
PASADENA, CALIFORNIA

July 1, 1965

Copyright © 1966
Jet Propulsion Laboratory
California Institute of Technology

Prepared Under Contract No. NAS 7-100
National Aeronautics & Space Administration

FOREWORD

Late in 1964, the *Voyager* Project received formal recognition from the National Aeronautics and Space Administration in the form of a Project Approval Document, enabling the establishment of a *Voyager* Project Office at the Jet Propulsion Laboratory to begin preliminary studies of *Voyager* spacecraft. At that time there was no formal authorization for the establishment of a *Voyager* capsule organization within the Laboratory. However, previous internal studies at JPL and by industry for the *Mariner* systems and for advanced planetary spacecraft systems had considered capsule landing systems for Mars.

Early in 1965, the JPL Advanced Technical Studies Office agreed to support the *Voyager* effort by studying several discrete problem areas relating to capsule technology which previous system studies had shown were most crucial. The particular areas of investigation that were to be studied in considerable depth are as follows:

1. Capsule delivery techniques
2. Capsule shape
3. Engineering models of the Martian atmosphere and surface
4. Relay-link descent-phase telecommunications
5. Descent and landing operations
6. 1971 landed science experiments
7. Power systems for a landed capsule

During the period of February through June, 1965, personnel from both the *Voyager* Project Office and the Office of Advanced Technical Studies coordinated their efforts in considering the above problems. This document is an interim report of what will be a continuing effort for many years to come. It was deemed important to document the results of study at this time, even though results are not complete, in order that the information generated to date would be generally available for comment, suggestion, and criticism. It is hoped that by examining areas heretofore unexplored, the reports in this series will stimulate the reader to communicate with the authors so that information and conclusions presented can be updated and improved as the *Voyager* program evolves.

CONTENTS

I. Introduction	1
II. Models of Mars' Atmosphere	2
A. Atmospheric Surface Density	2
B. Atmospheric Surface Pressure	2
C. Atmospheric Temperature Distribution	4
D. Atmospheric Composition	8
E. Martian Atmospheric Winds	8
F. Summary of Engineering Models of Mars' Atmosphere	12
III. Surface and Terrain Models of Mars	14
A. Bright Areas	14
B. Dark Areas	16
C. Summary of Engineering Models of Mars' Surface and Terrain	19
Nomenclature	20
Glossary	21
References	22

TABLES

1. Comparison of CO ₂ abundance w in m atm at 300°K; average Mars temperature = 230°K	3
2. Mars' surface pressure, mb	3
3. Cloud motions—periods and times observed	9
4. Minimum horizontal wind velocity as a function of altitude required to initiate grain motion on a rough desert (optimum particle size); surface pressure = 25 mb	10
5. Horizontal wind velocity as a function of altitude required to initiate motion of 50 μ particles for various surface roughnesses; surface pressure = 25 mb	10

TABLES (Cont'd)

6. Horizontal wind velocity as a function of altitude required to initiate motion of 50μ particles for various surface pressures and a surface roughness of $k_{R/5}$ 10

7. Properties of Mars' atmosphere, *Mariner 1969* models 11

8. Summary of Mars' surface characteristics and properties 19

FIGURES

1. Summary of Mars' surface-pressure interpretations 5

2. Wind direction relative to local slopes 12

3. Definition of normal and cross slopes 15

4. Diurnal surface temperature in bright area 16

5. Low-scale surface contour 17

6. Diurnal surface temperature in dark area 18

ABSTRACT

26871

Engineering models of the Martian atmosphere and surface are developed for application purposes in designing a Mars capsule-lander. Models are presented for various surface pressures and a number of low-altitude and stratospheric temperature profiles. An atmospheric surface pressure of 14 mb is suggested for design use. Mean continuous wind velocities of approximately 100 ft/sec at the surface are recommended, with a mean vertical gradient of plus 2 ft/sec/1000 ft. A peak design wind velocity of 330 ft/sec is recommended consistent with a 14-mb surface pressure. Models of Mars' surface are developed for the bright areas and the dark areas. The most significant differences in design requirements for these areas result from:

1. The convex and concave low-scale surface contours in the dark areas
2. Design requirement to accommodate 10-cm rocks in the dark areas

I. INTRODUCTION

The development of models of the Martian atmosphere and surface may result in significantly different models, depending on whether the model is required for the design of engineering subsystems or for scientific instruments. The Mars models presented in this report are developed solely for the purpose of estimating critical design conditions for a Mars capsule-lander. The Mars-atmosphere models are developed to encompass the "expected" worst conditions to be considered in the design of the capsule structure and heat shield, terminal deceleration subsystem (typically a parachute), and available descent time in the atmosphere. Separate engineering models of the Martian surface and terrain are developed for the bright areas and the dark areas in order to allow an engineering comparison of the difficulty in landing in either of these areas. The surface model is required in order to properly design the landing

energy absorber, to evaluate the dynamics of impact, and to evaluate the landed payload orientation and other payload support systems.

It should be understood that the amount of available observational data on the atmospheric and surface features of Mars is extremely limited. The Mars models are developed from ground-based observational data combined with analytical techniques to obtain nonobservable properties. Many of the physical properties and characteristics of Mars were estimated by considering (hopefully) analogous conditions on the Earth.

It is anticipated that these models will be updated as more information becomes available from ground-based observations of Mars and from the results of the *Mariner IV* occultation and photographic data.

II. MODELS OF MARS' ATMOSPHERE

A. Atmospheric Surface Density

The surface density of Mars' atmosphere is a critical quantity affecting the impact velocity of a descending capsule or terminal decelerator. To date, the observable effects lead to direct determination only of surface pressure, surface temperature (solid), and molecular weight of Mars' atmosphere. Therefore, surface density is a derived quantity from the observables through the equation of state.

B. Atmospheric Surface Pressure

The determination of the Martian atmospheric surface pressure and certain constituents of the atmosphere can be made from the analysis of photometric and polarimetric data or spectroscopic data obtained with large, properly instrumented ground-based telescopes. The earliest estimate of Mars' surface pressure, using polarimetric data, was made by Lyot in 1929. Lyot obtained a Martian surface pressure of 18 mb, assuming Mars' atmosphere to be composed of oxygen and nitrogen (Ref. 1). In the late 1940's and early 1950's, this method was updated by Dollfus, who attempted to determine the Martian surface pressure by combining polarimetric and photometric data. The polarimetric data compare the relative brightness (intensity) of scattered sunlight from Mars' atmosphere and surface, parallel and perpendicular to the plane containing the Sun, Mars, and Earth. The analysis assumes that the planet is a pure Rayleigh scatterer in the visible region of the spectrum. The polarimetric data are combined with photometric data (total intensity of reflected sunlight from the planet) to obtain an estimate of the Martian surface pressure.

Dollfus' original estimate yielded an atmospheric surface pressure of 90 mb, assuming the Martian atmosphere to be composed of air. This value has recently been revised to 62 mb if the atmosphere is composed of air. Using an argument similar to that of Dollfus, the authors of Ref. 1 calculate a surface pressure of 51 mb if the composition is one-third CO₂ and two-thirds N₂.

The method of Dollfus is suspect, however, since it is sensitive to scattering from any particles that may be present in the Martian atmosphere. To demonstrate this sensitivity, results shown in Ref. 1 indicate that the surface-pressure estimate may be in error by factors of 2 to 10. These results show that polarimetric and photo-

metric techniques in the visible spectrum should not be used to estimate the Martian surface pressure.

Recently, S. Musman (Ref. 2) has utilized the ultraviolet scattering data taken by G. de Vaucouleurs at 3300 Å to estimate an upper bound for the Martian surface pressure. Musman assumes the following:

1. The Martian atmosphere is free of strong absorption in the ultraviolet.
2. The atmospheric scattering follows a Rayleigh scattering law.
3. The surface albedo in the ultraviolet is negligible.

Musman estimates an upper limit to the Martian surface pressure of 27 mb if the atmosphere is 100 percent N₂, 19 mb if the atmosphere is 100 percent CO₂, and 22 mb if the atmosphere is one-third CO₂ plus two-thirds N₂.

Including the effects of particulate scattering, the authors of Ref. 1 show that Musman's approach is much less sensitive to solid particles in the atmosphere and that the surface pressure would be in error by only a few millibars. In summary, these techniques do not lead to as conclusive results as do the spectroscopic data discussed below.

The estimates of the Martian surface pressure based on ground-based telescopic spectroscopic data rely on the single plate of the CO₂ absorption spectrum at 8700 Å obtained by Kaplan, Münch, and Spinrad (KMS) as reported in Ref. 3.

The interpretation of the Martian atmospheric surface pressure depends on the total amount of CO₂ in Mars' atmosphere. The CO₂ abundance is obtained from a reduction of the 8700 Å CO₂ rotational line data taken by KMS. In order to differentiate between the original estimate of Mars' surface pressure given in Ref. 3 by Kaplan, Münch, and Spinrad and other recent estimates, each variation from the KMS assumed value will be discussed separately.

Brooks (unpublished) has more thoroughly evaluated the geometry of the KMS observations and has revised the effective air mass (observed path length in Mars' atmosphere) upward from 3.6 (KMS) to 3.9. This change reduces the total CO₂ abundance estimate.

P. Swan (Ref. 4) has pointed out that the $J = 36, 38,$ and 40 CO_2 R-branch lines overlap the $J = 8, 10,$ and 12 lines used by Kaplan, Münch, and Spinrad to estimate the total abundance. Using D. Rank's R-branch data¹ (Ref. 5), the present author calculates an average line strength of the $J = 8, 10,$ and 12 lines, not including the overlap, of $\bar{S} = 0.026 \text{ cm}^{-1}/\text{km atm}$ at 300°K for an average Martian atmospheric temperature of 230°K (compared to $0.027 \text{ cm}^{-1}/\text{km atm}$ at 300°K given by KMS). Including the overlap, the average line strength \bar{S} is $0.0294 \text{ cm}^{-1}/\text{km atm}$ at 300°K for a Martian atmospheric temperature of 230°K . This increased line strength also reduces the total CO_2 abundance estimate.

P. Hanst (Ref. 4) has independently calibrated the 8700 \AA CO_2 R-branch line strength. Using the reduction given by Swan, the average line strength \bar{S} of the $J = 8, 10,$ and 12 lines, including the overlap with the $36, 38,$ and 40 lines, is $0.048 \text{ cm}^{-1}/\text{km atm}$ at 300°K . This calibration produces a significantly reduced CO_2 abundance.

T. Owens (Ref. 6) has empirically matched the 8700 \AA KMS absorption spectra with laboratory absorption-tube spectra. Owens does not obtain a line-strength intensity measurement, but does report a total CO_2 abundance in the Martian atmosphere ($w = 46 \text{ m atm}$ for an atmospheric temperature of 230°K).

Table 1 compares the CO_2 abundance estimates obtained from the various sources. The author's preferred value includes the Brooks effect, and the overlap of the $J = 36, 38,$ and 40 lines, and is based on Rank's data.

Although the data have not been published, a student of H. Spinrad's has also recalibrated the 8700 \AA CO_2 R-branch line strengths reported by Rank. The data

¹The R-branch line strength actually measured by Rank is an integrated value for all $J \geq 8$, and the line intensities are reported for a column of gas at standard conditions. The line strength used here (and by KMS) is referred to as a column of gas at 300°K and 1 atm pressure.

Table 1. Comparison of CO_2 abundance w in m atm at 300°K ; average Mars temperature = 230°K

1	2	3	4
KMS original	Hanst & Swan	Owens	Spencer preferred
55 ± 20	28 ± 13	46 ± 20	47 ± 20

are not too accurate, but appear to give a line strength within the accuracy of that of Rank. These data are being verified by additional experiments. The NASA Ames Research Center is also in the process of calibrating the 8700 \AA CO_2 R-branch line strength. E. Inn of Ames Research Center, in a private communication, indicates that their intensity measurements agree with Rank's to within 15%. These data also should be available in the near future.

In order to calculate the total Martian surface pressure, an additional independent source of spectroscopic data is necessary. The data used by KMS and Hanst are based on 2.05μ CO_2 absorption spectra taken by Sinton and Kuiper. The author's preferred data are based on the 1.57μ CO_2 absorption spectra taken by Kuiper at a time when the Martian lines were doppler-shifted from the telluric absorption lines.

Using the same procedure described in Ref. 3, the Martian surface pressure has been recalculated for various combinations of CO_2 abundance and total pressure-broadened data (1.57μ and 2.05μ data). The results of the calculations are presented in Table 2 (columns B, E, and F), as well as the surface-pressure estimates of KMS, Kuiper, and Swan.

The surface-pressure estimate that is consistent with the combination of G. Kuiper's 1.57μ data and the revised CO_2 abundance is given in column F and is the author's preferred Martian surface-pressure estimate. A surface pressure of 17 mb should be considered to be a nominal surface pressure, not a mean surface pressure. Since astronomers tend to overestimate the amount of absorption indicated on the plates, it is more likely that the

Table 2. Mars' surface pressure^a, mb

A	B	C	D	E	F
KMS original	KMS, revised by Spencer	Kuiper	Swan	Swan, revised by Spencer	Spencer preferred
($1^b + 2.05\mu$ data)	($4^b + 2.05\mu$ data)	($3^b + 1.57\mu$ data—empirical)	($2^b + 2.05\mu$ data)	($2^b + 1.57\mu$ data)	($4^b + 1.57\mu$ data)
25 ± 15	29 ± 15	17 ± 3	53 ± 29	$31 + 29 - 12$	$17 + 19 - 9$
^a All estimates depend on single plate taken by Kaplan, Münch, and Spinrad, and average atmospheric temperature on Mars of 230°K . ^b Number corresponds to CO_2 abundance given in Table 1.					

mean Martian surface-pressure estimate would be greater than 17 mb.

The results presented in Table 2, as well as the results of the IITRI review (Ref. 1), are summarized in Fig. 1 together with the lower bounds on the Martian surface pressure if the atmosphere were 100% CO₂. The lower bounds were independent estimates by Dr. Hyman Spinrad and the author.

It is interesting to note that there is a range of Martian surface pressures consistent with all interpretations of the spectroscopic data (except G. Kuiper's 17 ± 3 mb, where the 3 mb is estimated to be a 1σ deviation) between 24 and 36 mb. Based on a statistical interpretation of the data (not a statistical set of data) it appears that the mean surface pressure would be somewhere in the range between 24 and 36 mb.

The previously discussed estimates were given for a mean atmospheric temperature of 230°K. Also shown in Fig. 1 is the effect of a lower mean temperature of 200°K. If the average atmospheric temperature were 200°K, the nominal surface pressure would be 1 to 2 mb higher than that estimated for a mean temperature of 230°K.

At this time, it is recommended that the entry capsule be designed consistent with a Martian surface pressure of 14 mb. This surface pressure is not an absolute lower bound, but represents a compromise that considers uncertainties in surface pressure as only one possible cause of capsule-lander failure. As will be discussed in Section IIC, the atmospheric surface temperature for terminal descent is assumed to be 300°K. Since density is the critical parameter affecting terminal descent velocity, the combination of a 14-mb surface pressure with a 300°K atmospheric surface temperature provides some density contingency should the surface pressure be 10 mb and the atmospheric surface temperature 207°K.

In addition to the minimum-surface-pressure models, model atmospheres using surface pressures of 25 mb (mean) and 40 mb (maximum) should also be used in order to determine the effects on capsule-lander design.

C. Atmospheric Temperature Distribution

Since most of the pertinent aerodynamic systems are functions of pressure or density at a particular altitude, the temperature distribution in the atmosphere must also be specified. The temperature distribution in the

lower atmosphere is most frequently described by an adiabatic lapse rate, i.e., rate of decrease in temperature with height, which cannot be exceeded for long without causing convective mixing. This approach predicts a lower bound on the temperature distribution in the atmosphere for a given atmospheric surface temperature. The maximum temperature at a given altitude is obtained by assuming the atmosphere is isothermal at the same value as the atmospheric surface temperature. Recently, various Martian temperature distributions have been developed between these extremes by G. Ohring (Ref. 7).

Y. Mintz (Ref. 8) has shown that the temperature of the atmosphere at the surface of Mars may be less than that of the solid surface, and the temperature difference depends on the diurnal variation of surface temperature. The larger the diurnal variation of the surface temperature, the greater the difference between the atmospheric and solid-surface temperatures. The maximum temperature difference between the solid surface and atmosphere at the surface is given by (Ref. 8)

$$T_{max}^s - T_{max}^a = 0.54 (T_{max}^s - T_{min}^s) \quad (1)$$

The minimum atmospheric surface temperature is somewhat higher than the minimum solid-surface temperature. This difference results from the large amount of heat lost by night emission from the solid surface as contrasted to the small amount of energy exchange from the ground and "night sky" and the atmosphere.

It has been found that the worst-case temperature model for a given surface pressure is not easily defined. In fact, it has been found that the worst-temperature distribution is highly dependent on the terminal descent mode selected. A discussion of the various worst-case temperature profiles follows.

1. Terminal Descent

When no terminal decelerator is used or after the terminal decelerator is deployed, the highest atmospheric surface temperature is the worst case. This results since the terminal descent velocity is inversely proportional to the square root of the local atmospheric density. For a given surface pressure, the atmospheric density is a minimum, producing a maximum impact velocity, if the atmospheric temperature of the surface is a maximum.

Based on ground-based determinations of Mars' solid-surface temperature, the maximum solid-surface temperature on Mars is 322°K (dark region). Assuming a

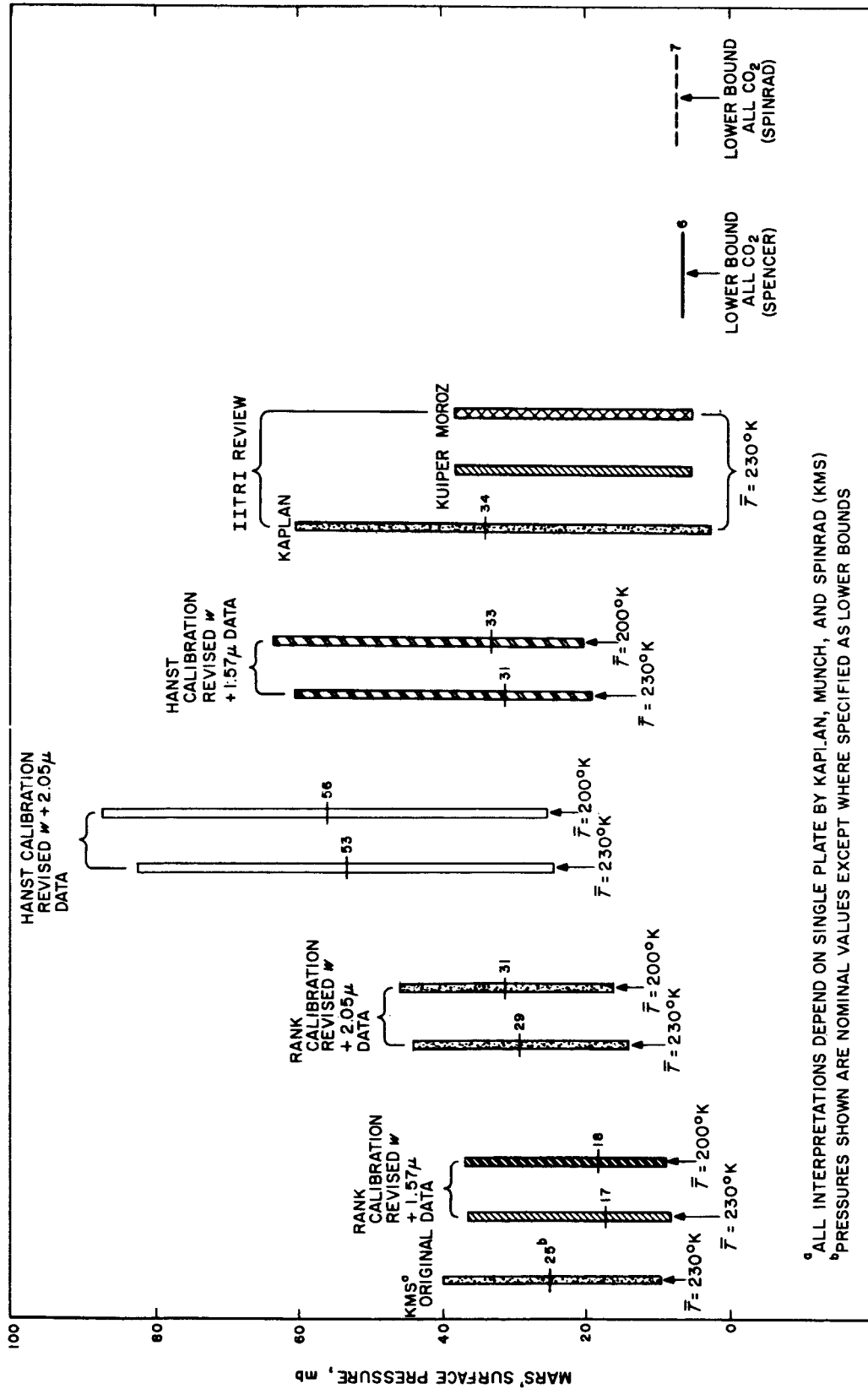


Fig. 1. Summary of Mars' surface-pressure interpretations

maximum diurnal variation of approximately 127°K, Eq. (1) predicts a difference between the solid-surface and surface atmospheric temperature of 69°C. The maximum atmospheric surface temperature predicted by using the Mintz approach (Ref. 8) is 253°K. *It is uncertain whether this approach is exact; therefore, the maximum atmospheric temperature at the surface for design purposes is recommended to be 300°K.* This temperature corresponds to a midday temperature near Mars' equatorial regions, during local summer, and for Mars at perihelion (approximate conditions for arrival in the southern hemisphere in 1971). The maximum temperature varies significantly with local time of day, latitude on Mars, and the radial distance of Mars from the Sun at encounter.

It is possible to weight the relative fraction of Mars' surface that would have this maximum temperature; however, with the limited data it is impossible to determine these fractional areas. If a specific landing site were selected and the landing dispersions were ±500 km (±7½ deg in latitude and longitude) it might be possible to reduce the maximum expected temperature.

2. Initiation of Parachute or Other Decelerator Sequence

In this case, the worst condition is a minimum atmospheric surface temperature. For decelerator initiation, the criterion is generally a Mach number (velocity) at a given altitude (pressure). From linear entry theory, the velocity of the entry body and local ambient pressure are related by

$$p(h) = 2g \Delta \sin \theta \ln \frac{V_e}{V(h)} \quad (2)$$

where

- $p(h)$ = the ambient pressure at altitude h , lb/ft²
- g = Mars' acceleration of gravity, 12.3 ft/sec²
- Δ = entry-capsule ballistic coefficient, slugs/ft²
- θ = entry angle, assumed constant over flight path, deg
- V_e = capsule-entry speed, ft/sec
- $V(h)$ = capsule speed at altitude h , ft/sec

Now, specifying a Mach number (velocity) required for decelerator deployment and a capsule ballistic coefficient, the ambient pressure $p(h)$ may be determined from Eq. (2).

The pressure as a function of altitude is given by

$$p = p_0 \left[1 - \frac{|\Gamma| h}{T_0} \right]^x \quad (3)$$

where

- $x = Mg/|\Gamma| R > 1$
- T_0 = atmospheric temperature at surface, °K
- Γ = adiabatic lapse rate, °K/km
- h = altitude, km
- M = molecular weight of atmosphere, gm/gmole
- R = universal gas constant, 830 dyne km/gmole °K
- g = Mars' acceleration of gravity, 375 cm/sec²

Solving Eq. (3) for the altitude at which the pressure is p yields

$$h \text{ at } p = \frac{T_0}{|\Gamma|} \left[1 - \left(\frac{p}{p_0} \right)^{1/x} \right] \quad (4)$$

It can be seen from Eq. (4) that the lowest value of the atmospheric surface temperature will yield the lowest (worst-case) deployment altitude for a fixed surface pressure and composition of the atmosphere².

For arrival at southerly latitudes in 1971, the minimum solid-surface temperature is 190°K. The minimum atmospheric surface temperature would be expected to be approximately this value or slightly higher for landing near the morning terminator. Since this environment represents a possible landing condition in 1971, *it is recommended that the terminal-descent deployment system be designed for an atmosphere with a 200°K surface temperature.*

It should be reiterated that these atmospheric temperatures pertain to landings within 40 deg of the equator during southern summer (Mars near perihelion). For landings later in the 1970s, Mars will be near aphelion. In the worst case, the temperature at the subsolar point may be 27°C less than when Mars is at perihelion. This will reduce the minimum atmospheric temperature even further.

²Actually Γ , the dry adiabatic lapse rate, is a weak function of temperature, but Γ only varies from -3.93°K/km to -3.83°K/km for extremes in atmospheric temperatures.

3. Maximum Loading and Total Radiative Heating During Entry

Again, from linear theory it may be seen that the maximum deceleration varies directly with the local inverse scale height:

$$a_{max} = \frac{\beta V_e^2 \sin \theta}{2e} \quad (5)$$

where

a_{max} = maximum deceleration, ft/sec²

e = base of natural logarithm

The local inverse scale height is defined as

$$\beta = \frac{gM}{RT} \quad (6)$$

Therefore, the atmospheric model that gives the minimum temperature at peak deceleration will produce the maximum aerodynamic loading on the capsule. The minimum stratospheric temperature is estimated theoretically to be approximately 100°K. For temperatures less than this value, the carbon dioxide in Mars' atmosphere would solidify and thereby be visible. Assuming an atmospheric surface temperature of 200°K, and a stratospheric temperature of 100°K connected by a dry adiabatic lapse rate of approximately -4°K/km, the lowest temperature at peak deceleration results. For most trajectories, the peak deceleration occurs above 25 km; therefore, the stratospheric temperature of 100°K will prevail (atmospheric temperature of the stratosphere is assumed isothermal at 100°K). *It is recommended that a stratospheric temperature of 100°K be used for design purposes, combined with an atmospheric surface temperature of 200°K.*

G. Ohring (Ref. 7) has recently finished a theoretical study of the temperature distribution in the atmosphere of Mars. The minimum temperature calculated by Ohring, assuming a surface temperature of 200°K, is 116°K at an altitude of 40 km. S. Hess (Ref. 9) states that the temperature at the tropopause may be as low as -160°C (113°K), but that the stratospheric temperature is probably -100°C (173°K). Thus, the 100°K isothermal stratospheric temperature is conservative.

It may be shown that the total integrated radiative heating of the entry capsule is also a direct function of β :

$$q_r \propto \beta^b \quad (7)$$

where

q_r = integrated radiative-heat load to the capsule

b = positive exponent

Radiative heating of the capsule occurs in the stratosphere; thus, the entry capsule experiences maximum total radiative heating for the same atmospheric model that produces maximum loading, i.e., a stratospheric temperature of 100°K.

4. Maximum Convective Heating

The total convective-heating input to the entry capsule can be shown to be inversely related to β :

$$q_c \propto \beta^{-c} \quad (8)$$

where

q_c = integrated convective-heat load to the capsule

c = positive exponent

Since convective heating of the capsule occurs primarily in the stratosphere, the maximum stratospheric temperature maximizes the total convective heating of the capsule. The absolute maximum value would result if the atmosphere were assumed to be isothermal at 300°K; however, this condition appears to be too conservative. *It is recommended that the maximum stratospheric temperature be assumed to be 260°K. This value should be used in conjunction with a 300°K surface temperature to define the maximum-temperature atmospheric model.*

G. Ohring (Ref. 7) also considers an atmospheric temperature profile based on a 300°K surface temperature. Ohring's results indicate that the stratospheric temperature would be 151°K at 56 km. The 260°K stratospheric temperature, therefore, appears to be a conservative maximum value.

Since the total radiative heating varies directly with the inverse scale height, and the total convective heating

varies inversely with the inverse scale height, it is impossible to select, a priori, the stratospheric temperature which maximizes total (convective plus radiative) heating. Current JPL analyses indicate that radiative heating dominates convective heating in a large (16-ft-diam.) capsule at a 90-deg entry angle and an entry velocity of 25,000 ft/sec. For lower entry velocities, convective heating may again predominate. If convective heating predominates, an entry angle of 20 deg will produce maximum total heating.

D. Atmospheric Composition

The only major constituent of the Martian atmosphere that has been positively identified is carbon dioxide. The total amount of CO₂ in the Martian atmosphere is estimated to be 47 m atm. This total amount of CO₂ corresponds to a partial pressure at the surface of 3.4 mb and produces an atmospheric surface pressure of 17 mb. The recommended surface pressure for design is 14 mb. This pressure corresponds to 55 m atm of CO₂ or 3.95 mb of CO₂. To obtain the total pressure of 14 mb, it is assumed that the other major constituent of the atmosphere is nitrogen. Thus, at this time the recommended composition for design is 20% by volume (28.2% by weight) CO₂ and 80% by volume (71.8% by weight) N₂ for a total surface pressure of 14 mb. For other Mars' atmospheric surface pressure models, the atmospheric composition will differ from that given above. This results from the fact that a different total abundance of CO₂ and a different amount of N₂ must be assumed to obtain different surface pressures.

It should be mentioned that the maximum radiative heating rate occurs for CO₂, N₂ mixtures of 15 to 20% CO₂ by volume. This maximum radiative heating results from the cyanogen formed in a shocked gas of CO₂ and N₂. The principal radiation is emitted in the cyanogen violet band with a lesser contribution from the cyanogen red band.

In the past, certain atmospheric models of Mars have contained rather large fractions of argon. The presence of some argon in the Martian atmosphere is almost a certainty, but large amounts of argon are no longer in vogue with astronomers. The basis for the large estimates once proposed was that the surface of Mars was composed of as much potassium-40 per unit area as the Earth's surface. The potassium-40 supposedly was deposited in the same relative abundance on Mars as on Earth during the formation of the planet. Potassium-40 undergoes positron decay with a 1.4×10^9 -year half life

to form argon-40, a stable isotope. Assuming that Mars has the same amount of argon per unit area as the Earth, i.e., same partial pressure at the surface, there would be 5.0 mb of argon in the Martian atmosphere.

It should be noted that leaving out argon is not conservative. Shock-tube tests have indicated that both radiative and convective heat-transfer rates are increased for CO₂, N₂ mixtures with 20 to 30% argon. These rates are increased particularly at flight velocities greater than 25,000 ft/sec. However, for 1971 and 1973 Mars-entry missions, the entry velocities of interest are well below 25,000 ft/sec. In addition, it has been shown in Ref. 10 that the blackout interval during entry is somewhat longer in an atmosphere containing large (30% by volume) amounts of argon. The effect, however, is of second order and will only modify the time at which the capsule exits blackout by less than 1 sec. As a consequence, an atmospheric model with no argon is recommended.

Trace amounts of precipitable water, $14 \pm 7\mu$ total abundance, and a maximum oxygen content of 70 cm atm were also identified by Kaplan, Münch, and Spinrad (Ref. 3) in the Martian atmosphere. None of these molecules is in sufficient abundance to affect capsule design.

E. Martian Atmospheric Winds

The only two sources of information that can provide some evidence on the extent of Martian winds are observations of "yellow" clouds and theoretical calculations of the meteorology of Mars. The motion of yellow clouds has been evaluated most extensively by F. Gifford (Ref. 11-13). Gifford divides the yellow clouds into two groups: first, those that cause displacements or obscurations located roughly in the central portion of the disk and, second, those that produce displacements of the limb, or show up as terminator projections. The first type, which cause obscuration near the center of the disk, are probably initiated by wind-driven sand and tend to form in low latitudes (near the equator). The clouds may cover only a small fraction of the disk and last a few days; however, there have been occasions such as the great dust storm of 1956 when the entire planet was cloaked in yellow clouds for several weeks. The maximum velocity of this type of yellow cloud ever observed is 81 ft/sec (one observation in October, 1926). There have been five occasions when cloud motions between 30 and 40 ft/sec have been identified. The accuracy of these estimates is approximately $\pm 25\%$. There seems to be evidence that low-level yellow clouds originate in

regions of higher surface temperature than do the limb projections. This is consistent with the hypothesis that the first type of yellow clouds are desert sand and dust storms. Thus, the Martian yellow clouds are presumably composed of wind-driven sand grains moving within a few meters of the surface of Mars, accompanied by an overlying dust cloud of much smaller particles extending to many thousands of meters. J. Ryan (Ref. 14) suggests a typical dust-cloud altitude of 6 km. Ryan's estimates of fall time for various-sized particles (1 to 100 μ) range from 4 hours (100 μ) to 300 days (1 μ) for a surface pressure of 25 mb. These times certainly bracket the observed cloud durations of 1 to 16 days (Ref. 12).

The second type of "yellow" cloud motions, the so-called limb projections, are also sometimes known as white clouds. These white clouds occur primarily in middle latitudes and probably represent aqueous condensation. The white clouds sometimes extend around the planet for a few thousand kilometers and exist for weeks. The maximum velocities of limb projections are 125 ft/sec (one observation in February, 1914) and 133 ft/sec (one observation in October, 1911). There have been two other observations, which yielded limb-projection motions of 81 and 70 ft/sec. Gifford states that the accuracy of these cloud-speed estimates is ± 40 to 50%. These limb projections have been reported to extend to very great elevations, 50 km at times, and have been observed to be completely detached from the Martian surface.

In order to develop a wind model for Mars' atmosphere, the average temporal occurrence of cloud drifts

of either type should be considered. An analysis of all of the data given in Ref. 12 has been made. In this analysis, the period of time during which cloud drifts of various velocities were observed on Mars, relative to the total period of time that Mars was viewed (assuming the planet was viewed daily) during a particular interval, near opposition, was obtained. All those oppositions where no cloud drifts were observed were discarded; therefore, the resulting frequency of cloud-drift events is overestimated.

The results of the comparison are given in Table 3. It is interesting to note that even with these relatively conservative fractions of time, cloud motions greater than 40 ft/sec are observed only 5% of the time and greater than 100 ft/sec only 1% of the time. If, in addition, it is assumed that surface-wind velocities great enough to form the clouds exist for at least 10% of the cloud lifetime³, an additional 2.5% of the time the velocities would be greater than 80 ft/sec (no matter what the surface pressure is). Therefore, wind velocity would be expected to be less than 40 ft/sec, 93% of the time. This relative frequency is based on the average cloud speed. If these values were approximately 50% low (maximum error stated by Gifford) the corresponding velocity would be 60 ft/sec. Gifford (Ref. 13) states that the average frequency is little more than one per opposition period (≈ 100 days). In other words, observations of cloud drifts are very infrequent events. It should be

³The 10% of cloud lifetime was added for all observed cloud drifts (including limb projections) and therefore is conservative.

Table 3. Cloud motions—periods and times observed

Terrestrial period	Fraction of time cloud motions observed	Fraction of time observed motion between limits, ft/sec					
		0-20	20-40	40-60	60-80	80-100	>100
July 2 to July 13, 1892 (12 days)	0.42	0.25	0.17	0	0	0	0
Oct. 6, 1911 to Jan. 16, 1912 (103 days)	0.14	0.08	0.02	0	0.02	0	0.02
Dec. 31, 1913 to Feb. 18, 1914 (50 days)	0.28	0.08	0.08	0.04	0	0.04	0.04
Jan. 24 to Jan. 29, 1915 (6 days)	0.67	0	0	0.67	0	0	0
Aug. 9 to Oct. 27, 1924 (80 days)	0.18	0.15	0.03	0	0	0	0
May 2 to May 29, 1937 (28 days)	0.32	0.32	0	0	0	0	0
Aug. 22 to Sept. 4, 1956 (14 days)	0.79	0	0.79	0	0	0	0
Time-average fractions	0.245	0.124	0.074	0.020	0.007	0.007	0.014

noted that these speeds are based on gross cloud motions and may not represent actual planetary wind speeds on Mars.

Ryan (Ref. 14) has made a theoretical analysis of the wind speeds necessary to form the yellow clouds. He shows that there is a minimum drag velocity near the surface to produce grain motion. For a surface pressure of 14 mb, the minimum velocity occurs for a grain particle size of 700μ and at 25 mb, the minimum velocity occurs for a particle size of 600μ . The minimum horizontal wind velocity required to produce grain motion is reproduced from Ref. 13 in Table 4 for a surface pressure of 25 mb.

As Ryan points out, it is believed that the sand grains on Mars have a diameter of 50μ ; therefore, higher velocities are required to produce grain motion. Ryan has considered values of surface roughness equivalent to the rougher terrestrial deserts, a second model being one-fifth as rough, and the third model being one-tenth as rough. In this case the velocity required to produce grain motion for a surface pressure of 25 mb is given in Table 5. If, as expected, the deserts on Mars are extremely smooth, the results given in the $k_{R/10}$ column should apply. Since the required velocity to cause grain motion is caused by drag on the particle, the results of the analysis for a surface pressure of 25 mb can be extrapolated down to 14 mb and up to 40 mb by assuming a constant dynamic pressure. These extrapolations yield the results shown in Table 6, assuming the surface roughness is $k_{R/5}$.

The significance of Table 6 lies in the fact that if the surface of Mars is covered by 50μ particles, the velocity at 1 m above the surface could be just less than 220 ft/sec for a surface pressure of 14 mb and no cloud motions would be observed.

Table 4. Minimum horizontal wind velocity as a function of altitude required to initiate grain motion on a rough desert (optimum particle size); surface pressure = 25 mb

h, m	$v(h), ft/sec$
1	87
10	110
100	133

If a less pessimistic case is taken, and the results given in Table 4 are extrapolated to a surface pressure of 14 mb, the velocity 1 m above the surface could be just less than 116 ft/sec and yet go undetected. In either case, a high horizontal wind at the surface could go undetected.

Based on these extremely limited facts, it is recommended that a continuous surface-wind speed 1 m above the surface be assumed to be equal to 116 ft/sec for a 14-mb surface pressure. As can be seen from the foregoing presentation, this certainly does not represent a maximum possible speed. The recommended continuous surface-wind speeds for other surface pressures from 7 to 40 mb are presented in Table 7. The recommended values of the continuous surface-wind speed are just below those required to cause saltation of optimum-diameter dust particles.

Superimposed on this surface-wind speed should be an increase in wind speed with elevation. The average gradient in the Martian atmosphere estimated by S. Hess

Table 5. Horizontal wind velocity as a function of altitude required to initiate motion of 50μ particles for various surface roughnesses; surface pressure = 25 mb

h, m	$v(h), ft/sec$		
	$k_{R/10}$	$k_{R/5}$	k_R
1	174	165	133
10	210	200	174
100	250	240	210
		Increasing roughness \blacktriangleright	

Table 6. Horizontal wind velocity as a function of altitude required to initiate motion of 50μ particles for various surface pressures and a surface roughness of $k_{R/5}$

h, m	$v(h), ft/sec$		
	$p_0 = 14 mb$	$p_0 = 25 mb$	$p_0 = 40 mb$
1	220	165	130
10	270	200	160
100	330	240	200

Table 7. Properties of Mars' atmosphere, Mariner 1969 models

Property	Symbol	Dimensions	M69-1	M69-2	M69-3	M69-4	M69-5	M69-6	M69-7	M69-8	M69-9	M69-10	M69-11	M69-12	
Surface pressure	p_0	mb	25	14	7	7	14	14	25	40	40	14	14	25	
		lb/ft ²	52.2	29.2	14.6	14.6	29.2	29.2	52.2	83.5	83.5	29.2	29.2	52.2	
Surface density	ρ_0	(gm/cm ³) 10 ⁵	2.92	2.10	1.65	1.10	1.74	1.74	2.92	4.55	4.55	2.62	2.62	4.38	
		(slugs/ft ³) 10 ⁵	5.66	4.08	3.20	2.13	3.38	3.38	5.66	8.84	8.84	5.09	5.09	8.49	
Surface temperature	T_0	°K	300	250	200	300	300	300	300	300	300	200	200	200	
		°R	540	450	360	540	540	540	540	540	540	360	360	360	
Stratospheric temperature	T_s	°K	260	180	100	100	100	260	100	260	100	100	200	100	
		°R	468	324	180	180	180	468	180	468	180	180	360	180	
Acceleration of gravity at surface	g	cm/sec ²	375	375	375	375	375	375	375	375	375	375	375	375	
		ft/sec ²	12.3	12.3	12.3	12.3	12.3	12.3	12.3	12.3	12.3	12.3	12.3	12.3	
Composition		CO ₂ (by mass)	%	10.6	28.2	78.5	78.5	28.2	28.2	10.6	4.1	4.1	28.2	28.2	10.6
		CO ₂ (by vol)	%	7	20	70	70	20.0	20.0	7.0	2.6	2.6	20.0	20.0	7.0
		N ₂ (by mass)	%	89.4	71.8	21.5	21.5	71.8	71.8	89.4	95.9	95.9	71.8	71.8	89.4
		N ₂ (by vol)	%	93	80	30	30	80.0	80.0	93.0	97.4	97.4	80.0	80.0	93.0
Molecular weight	M	mol ⁻¹	29.1	31.2	39.2	39.2	31.2	31.2	29.1	28.4	28.4	31.2	31.2	29.1	
Specific heat of mixture	c_p	cal/gm-°C	0.243	0.229	0.183	0.191	0.228	0.234	0.241	0.246	0.245	0.225	0.228	0.240	
Specific heat ratio	γ		1.39	1.38	1.38	1.36	1.39	1.37	1.40	1.40	1.40	1.39	1.39	1.40	
Adiabatic lapse rate	Γ	°K/km	-3.68	-3.89	-4.88	-4.68	-3.93	-3.83	-3.71	-3.64	-3.65	-3.98	0	-3.73	
		°R/1000 ft	-2.02	-2.13	-2.68	-2.57	-2.16	-2.10	-2.04	-2.00	-2.00	-2.18	0	-2.05	
Tropopause altitude	h_T	km	10.8	18.0	20.5	42.7	50.9	10.4	53.9	11.0	54.8	25.1	0	26.8	
		kilo ft	35.6	59.2	67.2	140	167	34.1	177	36.1	180	82.4	0	87.8	
Inverse scale height (stratosphere)	β	km ⁻¹	0.0505	0.0781	0.176	0.176	0.140	0.0541	0.131	0.0492	0.0128	0.140	0.070	0.131	
		ft ⁻¹ × 10 ⁵	1.54	2.38	5.38	5.38	4.26	1.65	4.00	1.50	3.90	4.26	2.13	4.00	
Continuous surface-wind speed ^a	v	ft/sec	87	116	164	164	116	116	87	62	62	116	116	87	
Peak surface-wind speed ^a	v_{max}	ft/sec	250	330	470	470	330	330	250	200	200	330	330	250	
Design vertical wind gradient	$\frac{dv}{dh}$	ft/sec/1000 ft	2	2	2	2	2	2	2	2	2	2	2	2	

^aThe parameter has been scaled with surface pressure rather than surface density. The difference resulting from various surface temperatures will be small.

(Ref. 9) is $+4$ ft/sec/1000 ft for northerly latitudes near the equator. Y. Mintz (Ref. 15) states that the mean zonal winds of the middle and upper troposphere, at least in middle latitudes, will be westerly (west to east) in the winter hemisphere, and easterly in the summer hemisphere. It is difficult to define to what altitude this vertical wind gradient might exist. *Based on this discussion and the known vertical wind shears in the Earth's atmosphere, it is recommended that an average design wind-speed gradient of $+2$ ft/sec/1000 ft be used for altitudes to 50,000 ft.*

In considering the design problem associated with a Mars landing, it can be shown that the worst-case wind occurs parallel to the local surface. Therefore, the lander should be capable of successfully landing in a horizontal wind (relative to the local slope) directed up the slope, down the slope, or across the slope (see Fig. 2).

It is recommended that the terminal-descent subsystem be designed to accommodate gust velocities up to a 200-ft/sec step function from a zero ambient velocity at any altitude. It would not, however, seem reasonable to assume that this gust occurs during parachute opening. The other major effect of surface winds is the effect on the landed payload.

Since it appears that very high wind velocities are required to form the dust clouds, any landed spacecraft operating for a period of a month or more on the surface should be capable of withstanding these peak winds. *The peak velocities recommended for design are 330 ft/sec (worst-case Martian surface pressure of 14 mb), 250 ft/sec for a surface pressure of 25 mb, and 200 ft/sec for a surface pressure of 40 mb.* For short-duration missions of less than a month, the continuous wind speed (Table 7) for a given surface pressure should be used to determine wind loads on the lander.

Two additional facets of the problem discussed by Gifford (Ref. 13) are the following:

1. The apparent correlation of yellow clouds (winds) with perihelion opposition of Mars.
2. The latitude dependence of winds as evidenced by cloud motions.

Regarding item 1, Ref. 11 shows the following:

1. There was no evidence of yellow clouds reported at the near-perihelion oppositions of 1909 and 1939, even though 4500 images were taken in 1909 and 8500 in 1939 at Flagstaff alone (Ref. 16).

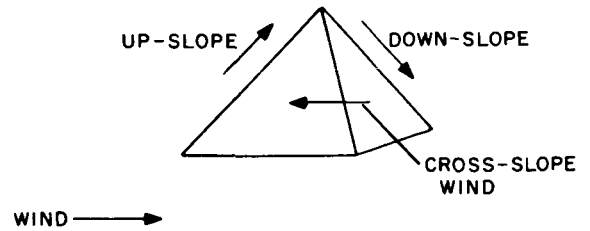


Fig. 2. Wind direction relative to local slopes

2. Large-scale cloud motions (velocities less than 25 ft/sec) were reported at the near-perihelion oppositions of 1924 and 1956.
3. Cloud motions have been observed at numerous non-perihelion oppositions. In fact, the maximum cloud velocities reported were in 1914 when Mars was nearer aphelion at opposition. These considerations indicate that there is no strong correlation with near-perihelion oppositions.

Regarding the latitude dependence of winds, all of the major cloud motions (velocities greater than 80 ft/sec) occurred below 10 deg north latitude, and occurred between local July and October in the southern hemisphere of Mars. Only one of the four occurrences of observed velocities greater than 80 ft/sec occurred at northern latitudes (during southern summer or fall). Arrivals in 1969 and 1971 will occur at approximately this local season. Although it appears that landings at northern latitudes would be somewhat less difficult, the same wind model should be utilized for landings anywhere on Mars.

In conclusion, it should be reiterated that the recommended wind model is based primarily upon observations of cloud motions and theoretical estimates of the velocities required to form the clouds. It is hoped that this investigation will stimulate other persons to objectively evaluate the data and perhaps suggest alternate interpretations. Also, other data that are pertinent to the evaluation of Martian winds should be obtained, if possible.

F. Summary of Engineering Models of Mars' Atmosphere

A series of model atmospheres for Mars have been developed from the preceding information. At the time the first of these model atmospheres was developed, the *Mariner 1969* mission was planned to include a Mars

entry probe or lander. Therefore, the designations of the atmospheric models given in Table 7 are M-69-i.

The model atmospheres include atmospheric surface pressure, surface density, surface temperature, stratospheric temperature, acceleration of gravity at the surface, composition, molecular weight, specific heat of mixture, specific heat ratio, adiabatic lapse rate, tropopause altitude, stratospheric inverse scale height, mean surface-wind speed, maximum surface-wind speed, and design vertical wind gradient.

The atmospheric models will be discussed in the order of increasing surface pressure. Model atmospheres M-69-3 and M-69-4 are based on the absolute lower-bound surface pressure of 7 mb. Model atmosphere M-69-3 provides the worst-case parachute-opening conditions, maximum aerodynamic loading, and maximum radiative heating. M-69-4 gives the maximum terminal-descent velocity at the surface. Neither model atmosphere M-69-3 nor M-69-4 is used for design purposes since these models appear to be too conservative.

Models M-69-2, M-69-5, M-69-6, M-69-10, and M-69-11 are based on a minimum surface pressure of 14 mb. Model M-69-2 is an average-temperature model. Model M-69-5 results in a maximum aerodynamic loading and radiative heating at 14 mb consistent with a maximum terminal-descent velocity at the surface. Model

M-69-6 results in maximum convective heating consistent with a maximum terminal-descent velocity at 14 mb. Model M-69-10 results in the most critical parachute-opening conditions (minimum pressure) at all altitudes and absolute maximum aerodynamic loading and radiative heating. Model M-69-11 combines the worst-case parachute-opening conditions with maximum convective heating consistent with a 200°K surface atmospheric temperature. The models based on a 14-mb surface pressure are presently used for design.

Models M-69-1, M-69-7, and M-69-12 are based on a mean Martian surface pressure of 25 mb. Model M-69-1 results in maximum terminal-descent velocity at the surface and maximum convective heating. Model M-69-7 results in maximum aerodynamic loading and radiative heating (at 25 mb) consistent with a maximum terminal-descent velocity. Model M-69-12 results in the worst-case parachute-opening condition, absolute maximum aerodynamic loading, and absolute maximum radiative heating.

Models M-69-8 and M-69-9 are based on a maximum surface pressure of 40 mb. Model M-69-8 produces maximum aerodynamic loading and radiative heating consistent with maximum terminal-descent velocity. Model M-69-9 produces maximum convective heating and maximum terminal-descent velocity.

III. SURFACE AND TERRAIN MODELS OF MARS

Engineering models of the Martian surface and terrain have been developed to enable the design of the energy-absorber system and landed-payload support systems. The models have been developed for two surface regions, the bright areas and the dark areas. The models should enable an engineering comparison to be made between landing system requirements in these areas.

It should be understood that the available amount of observational data on surface features of Mars is extremely limited. Most of the physical properties and characteristics of Mars' surface were estimated by considering analogous (hopefully) conditions on the Earth. An accounting has been made for the differences in surface gravity and atmospheric density between the Earth and Mars.

The models were developed to encompass most of the critical engineering-design conditions expected for a Mars lander. They are not absolute worst-case models; for example, they do not contain maximum-altitude mountains, fissures in the surface, 90-deg surface slopes, cavities that may exist in a lava flow, trees that might hang up a parachute, etc. It is expected that the fractional surface area covered by these extreme conditions is sufficiently small so that they may be neglected in an engineering model. Further, it would not appear necessary to design the lander for a surface condition that has a probability of one in a thousand, or less.

It is recommended that an independent evaluation of the surface and terrain engineering models be made to determine whether any major considerations were neglected in this study. In particular, a more thorough analysis of the physical properties of the surface should be made.

A. Bright Areas

1. General Characteristics and Features

The bright areas cover nearly three-fourths of the surface of Mars (Ref. 17) and are believed to be similar to our terrestrial deserts. Yellowish dust-veils over areas of Mars, sometimes on a planet-wide scale, provide evidence of dust or sand storms. Arguments presented (Ref. 13) state that the sand "dune-building winds on Mars are expected to be strong and persistent."

Available information on the bright areas is derived from photometric, polarimetric, colorimetric, infrared spectrometric, and radiometric measurements of the Martian surface. The bright areas of Mars show polarization curves very similar to those of the Moon. Therefore, it appears that the bright areas of Mars are covered with a dust very similar to the lunar surface (Ref. 17). It should be noted that G. de Vaucouleurs states that the lunar polarization curve is very similar to that obtained from terrestrial volcanic ash; however, he also states that "it would be very difficult to believe that the bright areas of Mars are actually covered with volcanic ash." However, both the polarimetric and infrared spectrophotometric results are in general agreement that the bright areas are composed of igneous material.

2. Composition

Based on the preceding discussion, the composition of the surface of Mars varies from limonite (see Glossary), or silicates with high contents of Fe_2O_3 , to feldspar, or volcanic ash. Kuiper matched the infrared spectrum of the bright areas of Mars to feldspar and states, "We may tentatively assume that the bright desert regions of Mars are composed of igneous rocks, similar to feldspar."

3. Relief

The relief must be fairly moderate since no permanent prominences have ever been observed to rise or set at the visible edge of the disk under oblique illumination, near the quadratures. If there are mountain ranges on Mars, they would not exceed 6,000 to 9,000 ft.

Although mountainous regions are not expected in the bright regions, the prospect of encountering sand dunes appears likely. Gifford (Ref. 13) has discussed the possibility of the Martian canals actually being sand dunes. The types of dunes may be either longitudinal dunes (called seif dunes) or crescent-shaped dunes (called barchan dunes). Gifford states that "the dune-building winds on Mars are expected to be strong and persistent"; thus the incidence of dune formation should be quite high.

It does not appear necessary to design for mountains of any altitude in the bright regions.

4. Slopes

Slopes are mainly determined by the shearing strength of the surfaces. Figure 3 defines the normal slope α_r and the cross slope δ .

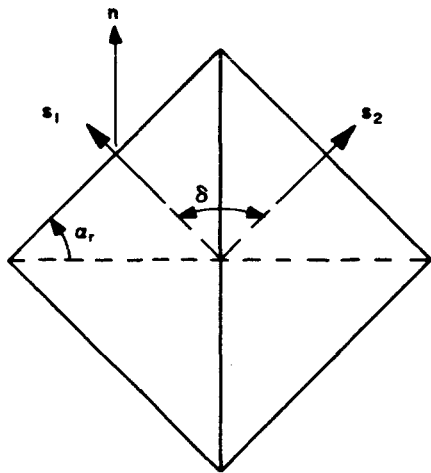
In the simple analysis of incipient slip, the angle of repose (normal slope) α_r can be assumed equal to the friction angle ϕ and is essentially independent of the planetary gravitational force.⁴ Since sand is essentially cohesionless, the shearing strength S of the surface is given simply by

$$S = P_e \tan \phi \tag{9}$$

where P_e is the effective pressure acting on the surface.

The friction angle at peak strength for loose, uniform, rounded sand is approximately 28 to 30 deg. The maximum possible value for dense, well-graded sand is 45 deg

⁴Actually, the pressure of the atmosphere would tend to decrease the friction angle slightly from the values given.



- s UNIT VECTOR NORMAL TO SLOPING PLANE
- n UNIT VECTOR ALONG NEGATIVE GRAVITY VECTOR
- α_r ANGLE OF REPOSE OF SLOPE
- δ ANGLE OF CROSS SLOPE

$$\alpha_r = \cos^{-1} (s_1 \cdot n)$$

$$\delta = \cos^{-1} (s_1 \cdot s_2)$$

Fig. 3. Definition of normal and cross slopes

(Ref. 18). It is recommended that the design slope be 0 to 30 deg.

5. Low-Scale Surface Contour

The low-scale surface contour refers to hemispherical undulations in the surface with radii of curvature from 10 cm to infinity. It should be realized that the surface features of Mars have not been resolved to better than 75 to 100 km, so that these variations must be assumed to be analogous to Earth-surface conditions.

Sand dunes in the bright area would be expected to have very large radii of curvature; therefore, the low-scale surface contour should not be important in the bright areas.

6. Surface Roughness

It is expected that the surface of the bright areas has been well weathered by wind-driven sandstorms. For engineering design purposes, a smooth surface on a 10-cm basis can be assumed. *The bright areas can be considered to be silty to coarse sand (5 μ to 2-mm-diam. particles).*

7. Surface Bearing Capacity

The ultimate surface bearing capacity of a cohesionless soil is a function of soil density or Mars unit weight, of the friction angle, and also the breadth of footing. The ultimate bearing capacity P_{ult} (Ref. 19) is as follows:

$$P_{ult} = K\lambda NB \text{ (lb/ft}^2\text{)} \tag{10}$$

where

K = a coefficient dependent on type of footing and can be assumed equal to 0.4

λ = specific weight of Mars' soil and equals 31 to 38 lb/ft³

N = bearing capacity factor and is a function only of ϕ (the value varies from approximately 5 to 10 for loose soils)

B = the breadth of the footing, ft

Then the ultimate surface bearing capacity of a typical loose, sandy Mars soil varies from 62 B lb/ft² (0.43 B lb/in.²) to 152 B lb/ft² (1.05 B lb/in.²).

The bright areas may, however, be hard, unyielding surfaces similar to the Great Plains. Therefore, an infinite bearing capacity in the bright areas must also be assumed.

8. Surface Temperature

The average surface-temperature variations on Mars are discussed by R. Newburn.⁵ In 1971, arrival in the southern hemisphere will be in early summer on Mars. The minimum diurnal surface temperature in the bright areas should be approximately 200°K for arrivals near the equator in 1971 (Mars near perihelion). The maximum diurnal surface temperature in the same region should be 310°K. The minimum surface temperature in the north polar regions appears to be nearly constant at about -70°C (≈ 200°K). Including measurement errors, the temperature may be as low as 195°K.

Therefore, the design surface-temperature environment should be a minimum temperature of 200°K in the equatorial region and a maximum temperature of 310°K (Model A in Fig. 4). The landed spacecraft should be capable, also, of handling the Model B (Fig. 4) diurnal temperature profile even though this condition is unlikely.

9. Other Physical Properties of the Surface

The density of the sand in the bright areas is approximately 1.3 to 1.6 gm/cc. Typical void fractions⁶ for dry

⁵The Environment in the Vicinity of the Surface of Mars, internal JPL communication, March 1, 1965.

⁶Void fraction is the volume of void divided by volume of solid.

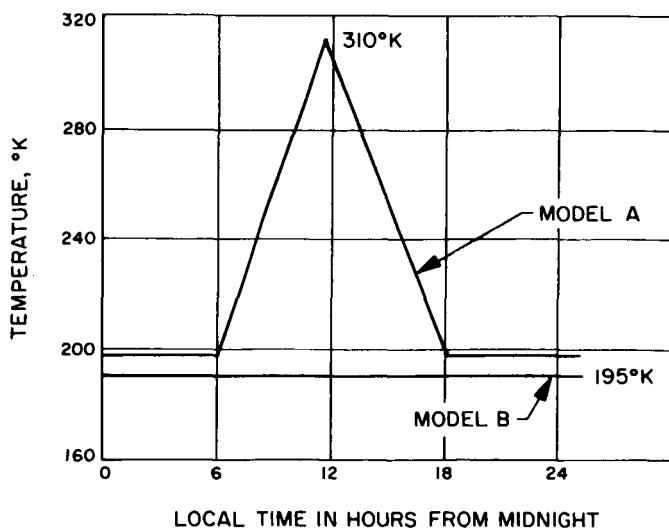


Fig. 4. Diurnal surface temperature in bright area

sand in the 5μ to 2-mm size range are 0.70 to 0.95 with porosities⁷ of 0.40 to 0.50.

Other surface properties such as specific heat, thermal conductivity, Mars' surface albedo for sunlight, and surface emissivity are necessary for a complete description of the surface. These variables are not critical to the lander design; however, they should be specified as part of an engineering-design model. Typical ranges of these properties are as follows:

Specific heat c_p , cal/gm°C = 0.15 to 0.50

Thermal conductivity k , cal/sec cm°C = 5×10^{-4} to 5×10^{-2}

Mars' surface albedo for sunlight $A = 0.15$ to 0.35

Average surface emissivity $\epsilon = 0.85$ to 1.0

B. Dark Areas

1. General Characteristics and Features

Although the dark areas cover only one-fourth of the surface of Mars, these are areas of extreme scientific interest from an exobiological standpoint, since they may harbor life. However, from an engineering-design standpoint, the dark areas should be assumed to be volcanic flows. These arguments stem from a consideration of the size of Mars relative to the Earth and the Moon. On both planets volcanism has played a major role in determining the present surface features (Ref. 20 and 21).

The structure and form of volcanoes varies markedly on the Earth depending on the amount of energy released, the magma viscosity, type of activity, etc. The major difference expected on Mars from an engineering-design standpoint is that the volcanic slopes⁸ can be greater than those on Earth due to the decreased gravitational force. In fact, volcanic slopes as large as 90 deg could be expected by extrapolating from Earth's gravity to Mars' gravity.

In the case of lavas of moderate viscosity, an aggregate of scoriaceous rounded fragments forms on the surface, and is often described as block lava, aa (pronounced ah-ah). For hot, mobile lavas, the surface skin forms a flat sheet with a coarse, streaky surface and is described as smooth pancake lava, or smooth pahoehoe (pronounced pa-hoy-hoy). Further, if the flow is retarded,

⁷Porosity is the volume of void divided by the total volume.

⁸The increased slopes result from the assumption that the magma viscosity is the same on the Earth and Mars.

the magma will be compressed in the direction of flow and thrown into folds, or so-called ropy lava. In general, it would be expected that the landed spacecraft might encounter any of these lava flow types.

2. Composition

The composition of the dark areas may vary from Earth-type vegetative matter to basaltic or felsitic lava flows. For engineering-design purposes, a siliceous rock varying in silica (SiO_2) content from 40 to 70%, alumina (Al_2O_3) from 1 to 18%, and magnesium oxide (MgO) from 46 to 1%, should be assumed (Ref. 9).

3. Relief

The dark areas of Mars might exhibit local high peaks. As pointed out by R. Newburn,⁹ isolated volcanic structures the size of Mt. Shasta (altitude 14,400 ft) would never be seen from Earth.

Although Mt. Shasta represents an extreme case on Earth, volcanic cones can easily be a few hundred feet to 25,000 ft above the mean surface level. Based on these arguments, it would appear that the landed payload should be capable of landing at a few thousand feet above the mean sea level. However, since conservative atmospheric temperature profiles have been used in conjunction with a low surface pressure (14 mb), it is recommended that this elevation effect not be included in the (surface) model.

The dark areas might exhibit relief very similar to the lunar surface. If the surface pressure is 10 to 25 mb, the number of meteoroid impacts on the surface will be much greater than on the Earth. In addition, the asteroid belt may produce a higher flux of large meteoroids at Mars. The craters formed by meteoroid impact would be expected to be partially filled by sand from wind-weathering not present on the Moon.

4. Slopes

Volcanic cinder cones are characterized by their steepness of slope (≈ 90 deg on Mars); however, they generally do not attain the areal extent of low-sloping lavas, so-called shield cones (maximum slope ≈ 22 deg on Mars). Most cones on Earth are intermediate between the two extremes. Since the cones themselves occupy a small area of a lava flow (typically 1 part in 10^4), the average slope encountered on Mars would be expected to be significantly less than the maximum slopes.

⁹Internal JPL communication.

Although meteoroid crater slopes can be as large as 90 deg, the fractional surface area of these high-slope conditions should be negligible. It would not appear necessary to design for crater-wall slopes.

It is recommended that the design slope for the dark areas be from 0 to 30 deg (direct and cross slope), as shown in Fig. 3.

5. Low-Scale Surface Contour

Undulations of the surface in the dark areas would be expected with radii of curvature in the range of 10 cm to infinity. Typical lava flows show both convex and concave hemispherical surface features with radii of curvature in this range (see Fig. 5). Therefore, the landed-payload energy-absorber should be capable of accommodating convex or concave surfaces of radii of curvature from 10 cm to infinity. However, it is not necessary to assume that the landed payload will hit directly in the center of a hole (concavity), or on a peak of a convex surface with a radius of curvature less than 2 times the radius of the landed-payload package.

6. Surface Roughness

The fragmental material (ejecta) surrounding a volcanic cone has varying shapes and characteristics. The largest pieces are blocks with dimensions ranging greater than 1 ft. Fortunately, these large blocks are concentrated near the cone peak. Smaller-size debris are bombs, cinders, and finally ash. The bulk of the material of the cone is, therefore, an accumulation of particles of continuous size range between cinders and blocks, whereas ash is the typical volcanic debris deposited primarily outside the periphery of the cone.

Most of the ejecta are smaller than 1 or 2 cm in diameter, although the debris may range up to objects 3 m in diameter. Debris surrounding Pigsaw crater in California shows that approximately 1% of the area is covered by pumice and cinders of 3 to 30 cm in diameter. Evaluation of the size distribution about Crater Lake in Oregon (Ref. 22) shows that only 1% of the debris had a diame-

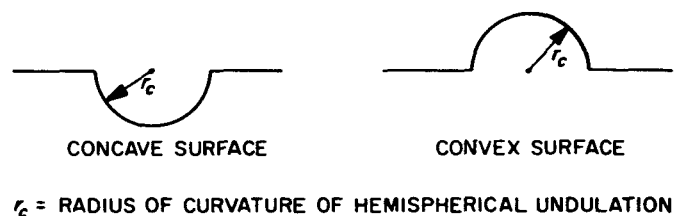


Fig. 5. Low-scale surface contour

ter greater than 6.4 cm. A similar evaluation of the debris about Oahu (Ref. 22) shows that 1% of the particles had diameters greater than 0.8 cm, and none had diameters greater than 1.6 cm.

As discussed in Ref. 22, the distribution of ejecta around various volcanoes indicates that some of the material has been segregated in part by the rate of settling through the Earth's atmosphere. Since Mars' atmospheric density is much more tenuous than the Earth's (1/25 to 1/100 that of the Earth) and the gravitational force is less, large-diameter debris would be expected to be spread over a larger area about the cone. In addition, those particles that form while cooling in their flight through the atmosphere should be larger in diameter on Mars than on Earth, since the aerodynamic ablation should be less. Based on this discussion, it would appear that 99% of the debris surrounding a typical crater would have diameters less than 10 cm.

Although the weathering of the ejecta (Ref. 23) has been neglected in the treatment, the lander should also be capable of landing on a flat area that may be covered with a thin (2 to 10 cm) layer of sand (100 μ particles) mixed with 1-mm to 1-cm particles of basalt. This condition would not appear to be as critical as those described above.

Therefore, it is recommended that the landing system be capable of accommodating a continuous surface made up of 10-cm rocks and that the system should also be capable of landing on a smooth (100 μ particles), hard surface.

7. Surface Bearing Capacity

The porosity of ejecta may vary from 0 to 50%, depending on the type of melt. *The more porous material has a relatively low bearing strength, the range in bearing strength being 1 to 10 psi.* The upper limit on the bearing capacity in the dark areas should be infinity. *The lander should be capable of accommodating bearing strengths between these extremes, as well as the range required for landing in a bright area.*

8. Surface Temperature

The dark areas have a higher absorptivity for sunlight than the bright areas and, therefore, should be somewhat warmer than the bright areas under insolation. A comparison of radiometric data of Mars (Ref. 17) shows that the temperature in the dark areas under insolation will be approximately 12°C higher than in the bright areas. Therefore, assuming the profile developed for the bright

areas (Fig. 4), the maximum temperature of the dark areas will be taken as 322°K at noon local time. This value should certainly be conservative.

Conversely, the dark areas should become somewhat colder than the bright areas at night, since the emissivity of the dark areas should be 0.95 to 1.0 in the infrared. Assuming an emissivity of 0.9 for the bright areas and 1.0 for the dark areas, the dark areas should be approximately 5°C colder than the bright areas during a Mars night; for this case, the minimum surface temperature of a dark area near the equator (within 40 deg latitude) is 190°K. *The recommended engineering-design models of the diurnal temperature for the dark areas are given in Fig. 6.* Model A represents the maximum expected temperature regime. Model B assumes an isothermal surface temperature 5°C colder than the bright areas. These two models should be utilized for design of lander temperature control in a dark area.

9. Other Physical Properties of the Surface

The density of the dark-area surface (assuming the material to be of volcanic origin) should range from 1.2 gm/cc (pumice, 50% porosity) to 2.6 gm/cc for compact, solid material. Other physical property ranges are:

Specific heat c_p , cal/gm°C (basalt to quartz) = 0.15 to 0.30

Thermal conductivity k , cal/cm sec°C = 2×10^{-4} to 4×10^{-3}

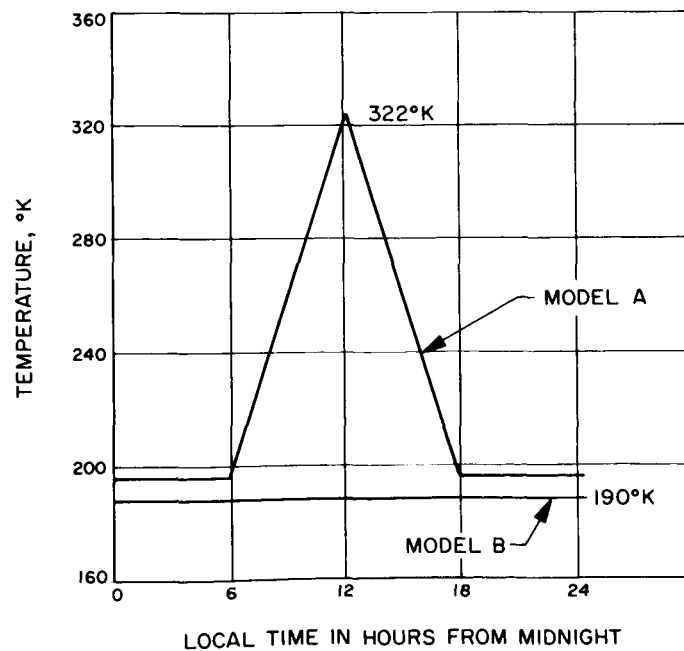


Fig. 6. Diurnal surface temperature in dark area

Average surface albedo for sunlight $A = 0.05$ to 0.25

Average surface emissivity $\epsilon = 0.95$ to 1.00

1. The convex and concave low-scale surface contour in the dark areas
2. Design requirement to accommodate 10-cm rocks in the dark areas

C. Summary of Engineering Models of Mars' Surface and Terrain

Table 8 contains a summary of the surface features of Mars for the bright and dark areas.

The most significant differences in design requirements for the bright and dark areas result from:

Based on a qualitative evaluation of these differences, it appears that designing a Mars lander for the dark areas is significantly more difficult than designing for the bright areas. Present scientific desires for landings in the dark areas and expected capsule-landing dispersions require that the lander design be capable of accommodating either terrain.

Table 8. Summary of Mars' surface characteristics and properties

Feature	Bright area	Dark area	Recommended design requirement
1) Fractional area of Mars' surface	0.75	0.25	Both regions
2) Composition	Limonite to silicates with high contents of $Fe_2O_3^a$	Siliceous rocks with 40 to 70% silica, 1 to 18% alumina, 1 to 46% magnesia	Full range of surface compositions
3) Relief	Low-elevation sand dunes	General low elevation with locally high (>10,000 ft) peaks	Zero elevation
4) Slopes, deg	0 to 45	0 to 30 Local slopes of 90	0 to 30
5) Low-scale surface contour	Effectively infinite radius of curvature	Convex and concave surfaces with radii of curvature between 10 cm and infinity	Convex and concave surfaces with radii of curvature between 10 cm and infinity. No landing on peak or hole with a radius of curvature less than 2 times the radius of the landed payload package
6) Surface roughness	5μ to 2-mm-diam. sand particles	Coarse (100- μ -diam.) sand to 10-cm-diam. rocks	Both surface roughnesses
7) Surface bearing capacity, psi	$0.43 B^b$ or $1.05 B$ to infinity	1 to infinity	Both regions
8) Surface temperature, °K	310 — Maximum 195 — Minimum	322 — Maximum 190 — Minimum	Both models A and B given in Fig. 4 and 6
9) Surface density, gm/cc	1.3 to 1.6	1.2 to 2.6	Both regions
10) Porosity	0.4 to 0.5	0.5 to 1.0	Both regions
11) Specific heat, cal/gm°C	0.15 to 0.50	0.15 to 0.30	Both regions
12) Thermal conductivity, cal/cm sec °C	2×10^{-1} to 4×10^{-3}	5×10^{-1} to 5×10^{-2}	Both regions
13) Average surface albedo for sunlight	0.15 to 0.35	0.05 to 0.25	Both regions
14) Average surface emissivity	0.85 to 1.0	0.95 to 1.00	Both regions

^aSee glossary for typical composition.

^bBreadth of footing in feet.

NOMENCLATURE

<i>A</i> surface albedo, dimensionless	<i>x</i> dimensionless exponent (defined in text)
<i>a</i> acceleration, ft/sec ²	<i>α_r</i> angle of repose, deg
<i>B</i> breadth of footing, ft	<i>β</i> inverse scale height, ft ⁻¹ or km ⁻¹
<i>b</i> positive exponent	<i>Γ</i> adiabatic lapse rate, °K/km or °R/1000 ft
<i>c_p</i> specific heat, cal/gm °C	<i>γ</i> specific heat ratio, dimensionless
<i>c</i> positive exponent	<i>Δ</i> ballistic coefficient, slugs/ft ²
<i>e</i> base of natural logarithm	<i>ζ</i> angle of cross slope, deg
<i>g</i> Mars' acceleration of gravity = 12.3 ft/sec ² or 375 cm/sec ²	<i>ε</i> surface emissivity, dimensionless
<i>h</i> altitude, km or cm, or kilofeet	<i>λ</i> specific weight of Mars' soil, lb/ft ³
<i>J</i> rotational quantum number	<i>μ</i> micron
<i>K</i> coefficient dependent on type of footing, dimensionless	<i>ρ</i> density, gm/cm ³ , or slugs/ft ³
<i>k</i> thermal conductivity, cal/sec cm °C	<i>φ</i> friction angle, deg
<i>k_E</i> surface roughness parameter of typical terrestrial desert	
<i>M</i> molecular weight, gm/gmole or lb/lbmole	Subscripts
<i>N</i> bearing-capacity factor, dimensionless	<i>c</i> convective
<i>n</i> unit vector along negative gravity vector	<i>e</i> entry
<i>P_e</i> effective pressure, lb/in. ²	<i>max</i> maximum
<i>P_{ult}</i> ultimate bearing capacity, lb/ft ² or lb/in. ²	<i>min</i> minimum
<i>p</i> pressure, lb/ft ² or mb	<i>r</i> radiative
<i>q</i> integrated heat load, Btu/ft ²	<i>s</i> stratosphere
<i>R</i> universal gas constant = 830 dyne km/gmole °K	<i>T</i> tropopause
<i>r_c</i> radius of curvature, cm	<i>w</i> wind
<i>S</i> shearing strength, lb/in. ²	<i>0</i> zero altitude
\bar{S} average line strength, cm ⁻¹ /km atm	<i>1</i> first plane
<i>s</i> unit vector normal to sloping plane	<i>2</i> second plane
<i>T</i> temperature, °R or °K	
<i>V</i> capsule entry speed, ft/sec	Superscripts
<i>v</i> wind speed, ft/sec	<i>^a</i> atmosphere
<i>d\bar{v}/dh</i> mean vertical wind gradient, ft/sec/1000 ft	<i>^c</i> cross slope
<i>w</i> total abundance, m atm	<i>^d</i> down slope
	<i>^s</i> solid surface
	<i>^u</i> upslope
	$\bar{\text{—}}$ mean value

GLOSSARY

(In sequence of use)

1. Limonite: Approximately $2 \text{Fe}_2\text{O}_3 \cdot 3\text{H}_2\text{O}$ (iron 59.8%, oxygen 25.7%, water 14.5%); an amorphous, colloidal variety of hydrated iron oxide, which like hematite (Fe_2O_3), is extremely widespread as a coloring agent in rocks and soils. Often it is finely disseminated, but common occurrences are granular, porous masses of brown or yellow-brown color.
2. Hematite: Fe_2O_3 (iron 70%, oxygen 30%), which is the principal ore of iron and has a characteristic brown or cherry-red color.
3. Silicates with high contents of Fe_2O_3 : Characteristic of the Earth's crust and of the composition of average igneous rock (igneous rocks are products of melt generated within the planetary surface and subsequently ejected). Major constituents of a typical-composition igneous rock on the Earth are SiO_2 , 59.1%; Al_2O_3 , 15.3%; Fe_2O_3 , 3.1%; FeO , 3.8%; MgO , 3.5%; CaO , 5.1%; Na_2O , 3.0%; K_2O , 3.1%.
4. Felsite: A common igneous rock of orthoclase (aluminum and potassium silicate) with quartz grain in occlusion. The felsites are aphanitic in texture; i.e., rocks show the presence of variable amounts of glass as matrix.
5. Orthoclase: KAlSi_3O_8 ; $\text{K}_2\text{O} \cdot \text{Al}_2\text{O}_3 \cdot 6\text{SiO}_2$; silica, 64.7%; alumina, 18.4%; potassia, 16.9%.
6. Volcanic ash: Sandy fragments, consisting either of pulverized magma (glassy ash) or of pulverized rock material from the vent wall or a mixture of both. The composition can be assumed to be silicates with high contents of Fe_2O_3 .
7. Relief: The elevations or irregularities, collectively, of a land surface.
8. Pumice: Highly vesicular, highly porous, glassy, solidified magma fragments thrown out by violent explosions.
9. Magma: Silicate melt within (and beneath) the Earth's crust and in which are dissolved volatile constituents from which igneous rocks are formed.
10. Volcanism: Volcanic action including all natural processes at work in the formation of volcanoes.
11. Basalt: An igneous rock of greenish-black color.
12. Bomb: Solid matter near a volcanic cone formed by solidification of ejected molten material in the atmosphere.

REFERENCES

1. Cann, M. W. P., Davies, W. O., Greenspan, J. A., and Owen, T. C., *A Review of Recent Determinations of the Composition and Surface Pressure of the Atmosphere of Mars*, Final Report W6096, IIT Research Institute, Chicago, Illinois, March 15, 1965.
2. Musman, S., "An Upper Limit to a Rayleigh Scattering Atmosphere on Mars," *Planetary and Space Science*, Vol. 12, August 1964, p. 799.
3. Kaplan, L. D., Münch, G., and Spinrad, H., "An Analysis of the Spectrum of Mars," *Astrophysical Journal*, Vol. 139, No. 1, January 1964, pp. 1-5.
4. Hanst, P. L., and Swan, P. R., "The Absorption Intensity of the $5\mu_3$ Band of Carbon Dioxide and the Martian CO_2 Abundance and Atmospheric Pressure," *Icarus*, Vol. 4, September 1965, pp. 353-361.
5. Rank, D. H., Fink, U., Foltz, J. V., and Wiggins, T. A., "Intensity Measurements on Spectra of Gases of Planetary Interest— H_2 , H_2O , and CO_2 ," *Astrophysical Journal*, Vol. 140, No. 1, July 1964, pp. 366-373.
6. Owen, T. C., "A Determination of the Martian CO_2 Abundance," *Communications of the Lunar and Planetary Laboratory*, Vol. 2, Nos. 31-35, 1964, pp. 133-140.
7. Ohring, G., and Mariano, J. F., *Study of the Average Vertical Distribution of Temperature in the Martian Atmosphere*, Final Report GCA-TR-63-3-N, Geophysics Corporation of America, Bedford, Mass., March 1965.
8. Mintz, Y., "A Note on the Temperature of the Equatorial Troposphere of Mars," RM-2769-JPL, The Rand Corporation, Santa Monica, Calif., April 28, 1961, pp. 81-97.
9. Hess, S. L., "Some Aspects of the Meteorology of Mars," *Journal of Meteorology*, Vol. 7, No. 1, February 1950, pp. 1-13.
10. Spencer, D. F., *An Evaluation of the Communication Blackout Problem for a Blunt Mars-Entry Capsule and a Potential Method for the Elimination of Blackout*, Technical Report No. 32-594, Jet Propulsion Laboratory, Pasadena, Calif., April 15, 1964.
11. Gifford, F. A., Jr., "A Study of Martian Yellow Clouds That Display Movement," *Monthly Weather Review*, Vol. 92, No. 10, October 1964, pp. 435-440.
12. Gifford, F. A., Jr., *Interim Report on a Study of Martian Yellow Clouds That Display Movement*, August 2, 1963 (JPL internal document).
13. Gifford, F. A., Jr., "The Martian Canals According to a Purely Aeolian Hypothesis," *Icarus*, Vol. 3, 1964, pp. 130-135.
14. Ryan, J. A., "Notes on Martian Yellow Clouds," *Journal of Geophysical Research*, Vol. 69, No. 18, September 15, 1964, pp. 3759-3770.
15. Mintz, Y., "The General Circulation of Planetary Atmospheres," *Proceedings of the Lunar and Planetary Exploration Colloquium*, Vol. 3, No. 1, May 15, 1962, pp. 1-21.
16. Slipher, E. C., *The Photographic Story of Mars*, Sky Publishing Corp., Cambridge, Mass., 1962.
17. de Vaucouleurs, G., *Physics of the Planet Mars*, Faber and Faber Limited, London, 1954.
18. Tschebotarioff, G. P., *Soil Mechanics, Foundations, and Earth Structures*, McGraw-Hill Book Co., Inc., New York, 1951.

REFERENCES (Cont'd)

19. Hough, B. K., *Basic Soil Engineering*, Ronald Press Company, New York, 1957.
20. Urey, H. C., *The Planets, Their Origin and Development*, Yale University Press, New Haven, 1952.
21. Rittmann, A., *Volcanoes and Their Activity*, John Wiley and Sons, New York, 1962.
22. Dapples, E. C., *Basic Geology for Science and Engineering*, John Wiley and Sons, New York, 1959.
23. Sharp, R. E., "Wind-Driven Sand in Coachella Valley, California," *Geological Society of America Bulletin*, Vol. 75, September 1964, pp. 785-804.

ACKNOWLEDGMENT

The author is indebted to many individuals who were consulted in developing the models. In particular, conversations with Dr. Lewis Kaplan of JPL, Dr. Gerald Kuiper of the University of Arizona, and Dr. Paul Swan of Avco, regarding the Martian atmospheric surface pressure, were invaluable. Conversations with other members of the JPL staff, particularly Mr. J. Spiegel, Dr. R. Stephenson, Dr. P. K. Eckman, Dr. R. B. Brereton, and Mr. R. L. Newburn, were instrumental in bringing these models to their present form.

All conclusions presented in this report are those of the author, and while the assistance of those named here is gratefully acknowledged, it should not be assumed that they concur in these conclusions.